A Multi-Domain Connectome Convolutional Neural Network for Identifying Schizophrenia from EEG Connectivity Patterns

A Multi-Domain Connectome Convolutional Neural Network for Identifying Schizophrenia from EEG Connectivity Patterns

Chun-Ren Phang, Fuad Noman, Hadri Hussain, Chee-Ming Ting*, *Member, IEEE* and Hernando Ombao

***Abstract*—*Objective*: We exploit altered patterns in brain functional connectivity as features for automatic discriminative analysis of neuropsychiatric patients. Deep learning methods have been introduced to functional network classification only very recently for fMRI, and the proposed architectures essentially focused on a single type of connectivity measure. *Methods*: We propose a deep convolutional neural network (CNN) framework for classification of electroencephalogram (EEG)-derived brain connectome in schizophrenia (SZ). To capture complementary aspects of disrupted connectivity in SZ, we explore combination of various connectivity features consisting of time and frequency-domain metrics of effective connectivity based on vector autoregressive model and partial directed coherence, and complex network measures of network topology. We design a novel multi-domain connectome CNN (MDC-CNN) based on a parallel ensemble of 1D and 2D CNNs to integrate the features from various domains and dimensions using different fusion strategies. We also consider an extension to dynamic brain connectivity using the recurrent neural networks. *Results*: Hierarchical latent representations learned by the multiple convolutional layers from EEG connectivity reveals apparent group differences between SZ and healthy controls (HC). Results on a large resting-state EEG dataset show that the proposed CNNs significantly outperform traditional support vector machine classifier. The MDC-CNN with combined connectivity features further improves performance over single-domain CNNs using individual features, achieving remarkable accuracy of 91.69% with a decision-level fusion. *Conclusion*: The proposed MDC-CNN by integrating information from diverse brain connectivity descriptors is able to accurately discriminate SZ from HC. *Significance*: The new framework is potentially useful for developing diagnostic tools for SZ and other disorders.**

***Index Terms*—EEG, brain connectivity networks, deep learning, convolution neural networks, ensemble classifiers.**

I. Introduction

SCHIZOPHRENIA (SZ) is a major neuropsychiatric disorder. Neuroimaging studies have provided compelling evidences of both structural and functional brain abnormalities in SZ [1, 2]. Findings of structural magnetic resonance imaging (MRI) showed consistent decrement of brain tissues especially white matter in SZ patients [3]. Functional MRI (fMRI) studies had associated SZ with functional impairment in sensory and frontal brain areas [4]. Electrophysiological studies also reported shortening of electroencephalogram (EEG) microstates in fronto-central regions [5], and abnormalities of theta and gamma EEG oscillations related to memory impairment in SZ patients [6]. However, disruptions in the function of a single brain region cannot fully explain the range of various impairments observed in SZ. There is a need to identify altered connectivity between brain regions as a whole network.

Investigating brain connectivity networks based on neuroimaging data has become an important tool to understand the structural and functional organization of the human brain in health and disease. Alterations in the brain connectivity patterns have been associated with various neuropsychiatric disorders and are potentially useful as biomarkers for clinical applications. SZ is regarded as a dysconnectivity disorder characterized by abnormal structural and functional brain connectivity networks at both microscopic and macroscopic levels [7, 8]. Disconnection of white matter projection tracts has been observed in SZ patients [9–11] using MRI and diffusion tensor imaging (DTI). Analysis of functional connectivity (FC), the statistical dependencies between signals (fMRI or EEG) from spatially distant brain regions, has revealed dysconnectivity in schizophrenic brain networks especially between the frontal regions [8]. EEG studies reported SZ-related aberrant synchronization of neural oscillatory at both the low and high frequencies [12, 13]. However, the observed differences in FC patterns between SZ and controls have been inconsistent among fMRI studies, with reports of hyperconnectivity and hypoconnectivity (the increased and decreased strength of connections) between the same brain regions [9]. There are also contradictory findings from EEG studies reporting both increased [14] and reduced [15, 16] delta/theta band coherence, and both intact [15, 16] and reduced [17] beta-band connectivity in SZ. Complex network analysis based on graph theory [18, 19] has also revealed altered topological organization of brain connectome in SZ patients. Schizophrenic structural brain networks exhibits higher clustering, diminished overall connectivity strength and reduced global efficiency compared to healthy controls [10, 20]. The network topology of EEG-based connectivity in SZ has not yet been fully investigated.

Machine learning algorithms have been employed for automated classification of altered brain activity in SZ using EEG and fMRI data, primarily based on traditional classifiers such as support vector machine (SVM) [21–24], kernel discriminant analysis (KDA) [25] and adaptive boosting [26]. Moreover, most previous works on EEG-based classification of SZ used

C.-R. Phang, F. Noman and Hadri Hussain are with the School of Biomedical Engineering & Health Sciences, Universiti Teknologi Malaysia, 81310 Skudai, Johor, Malaysia (e-mail: phangcr@gmail.com).

C.-M. Ting is with the Medical Devices & Technology Centre, School of Biomedical Engineering & Health Sciences, Universiti Teknologi Malaysia, 81310 Skudai, Johor, Malaysia, and also the Statistics Program, King Abdullah University of Science and Technology, Thuwal 23955, Saudi Arabia (e-mail: cmting@utm.my).

H. Ombao is with the Statistics Program, King Abdullah University of Science and Technology, Thuwal 23955, Saudi Arabia (e-mail: hernando.ombao@kaust.edu.sa).

time-frequency features from single EEG channels such as band-specific spectral power and univariate autoregression model coefficients [26, 27]. The primary limitation of these single-channel approaches is that they ignore the interactions between channels as a network which has been shown to provide useful information in discriminating SZ from healthy controls at the group-level. Recent advances in deep learning techniques have been shown to be promising for neuroscience applications [28]. Deep neural networks (DNNs) have been used to classify brain connectivity of autism spectrum disorder (ASD) with encouraging accuracy [29–31]. Recent studies showed that DNN initialized with deep belief network outperformed SVM in classifying brain connectome of SZ [32, 33].

One popular DNN architecture, the convolutional neural networks (CNNs), has demonstrated superior capability of representing spatial patterns with remarkable success in classifying two-dimensional (2D) images [34]. This is well-suited to model brain connectivity networks with nodes arranged according to anatomical spatial proximity such as EEG channels. The CNNs, which alternately stack multiple convolutional layers and pooling or sub-sampling layers, can efficiently learn a hierarchy of latent representations that are invariant to small transitions of the inputs and allow for parameters sharing via its sparse localized kernels. Applications of CNNs to brain connectome data in classifying spatial maps of functional networks are introduced only recently and in its very early stage. A few related works include classification of fMRI-derived functional connectivity in mild cognitive impairment [35] and in resting-state networks [36], as well as DTI-based structural connectivity for predicting neurodevelopment in infants [37]. However, the convolutional architectures proposed in these studies focused on one type of connectivity measures from a single domain such as the Pearson correlation for functional connectivity, which did not take into account the connection directionality and topological organization of the brain networks. It remains a challenging task to integrate connectivity metrics from diverse domains (possibly with different dimensions) in the connectome CNNs. To our best knowledge, there are no prior studies using CNN for classification of EEG-based connectivity in SZ. Furthermore, we are not aware of any studies that investigated the classification performance of the combined low-level effective connectivity measures and the global-level complex network measures as input features.

The main contributions of this work are summarized as follows:

1) We propose a framework based on deep CNNs for classifying EEG-derived altered brain connectivity patterns in SZ.
2) We exploit, for the first time, effective brain connectivity, a generalization of FC with directionality of information flows between brain regions, as hand-crafted discriminative features in CNN for automatic classification of SZ. We examine various measures of directed connectivity estimated from EEG to capture disrupted brain network organization in SZ. These include the time-domain vector autoregressive (VAR) model coefficients, the frequency-domain partial directed coherence (PDC), the network topology-based complex network (CN) measures, and the combination of these connectivity features.
3) We design a novel deep CNN architecture called the multi-domain connectome CNN (MDC-CNN) that allows fusion of the time-domain, frequency-domain and topological measures of brain connectivity networks. The proposed CNN is an ensemble of two 2D-CNNs and one 1D-CNN combined in a parallel configuration, taking inputs of VAR, PDC and CN connectivity features, respectively. The MDC-CNN is able to learn latent hierarchical representations of the EEG network connectivity patterns with its deep convolutional layers, and then integrates complementary features of the connectivity strength, directionality and network topology to improve classification performance over conventional classifiers.
4) We examine different fusion strategies in the MDC-CNN in combining CNN classifiers trained on different domains of connectivity features: (1) feature-level fusion by concatenating feature maps of convolutional layers, (2) score-level fusion by concatenating activation outputs of the fully-connected layers, and (3) decision-level fusion by weighted average of predicted probabilities from independent classifiers trained on the VAR, PDC and CN features, respectively.
5) We extend the proposed framework to classify dynamic functional connectivity based on deep recurrent neural networks.

The paper is organized as follows: Section II describes the EEG connectivity features and the proposed MDC-CNN architectures. Section III reports classification performance on a large schizophrenia EEG dataset in comparison with conventional classifier, for different connectivity feature sets at main EEG frequency bands. Section IV draws the conclusion.

II. Methods

Fig. 1 shows an overview of the proposed MDC-CNN framework for classifying SZ and healthy control (HC) using EEG-based effective brain networks, which consists of two stages: connectivity feature extraction and CNN-based classification. In the first stage, various crafted measures of directed brain connectivity were estimated from multi-channel EEG: time-domain VAR coefficients, frequency-domain PDC and topological-based CN measures. In the second stage, The extracted connectivity features in different domains were then used as inputs to an ensemble of deep CNN classifiers. The two-dimensional connectivity matrices (i.e., VAR coefficient matrices at L lags and PDC matrices at five main frequency bands) are shaped into a 3D-tensor and taken as input to a 2D-CNN model. The one-dimensional vectors of concatenated CN features over five frequency bands were shaped into a 2D-tensor and used as input to a 1D-CNN. The convolution layers of CNN will further learn higher-level structural spatial features in the crafted connectivity measures. In the fusion of multiple CNN classifiers, resulting feature maps of different connectivity measures were flattened and combined, followed by fully-connected layers and a softmax layer to classify into SZ and HC. An alternative strategy is by weighted average of the decision scores from independent CNNs trained on different feature domains.

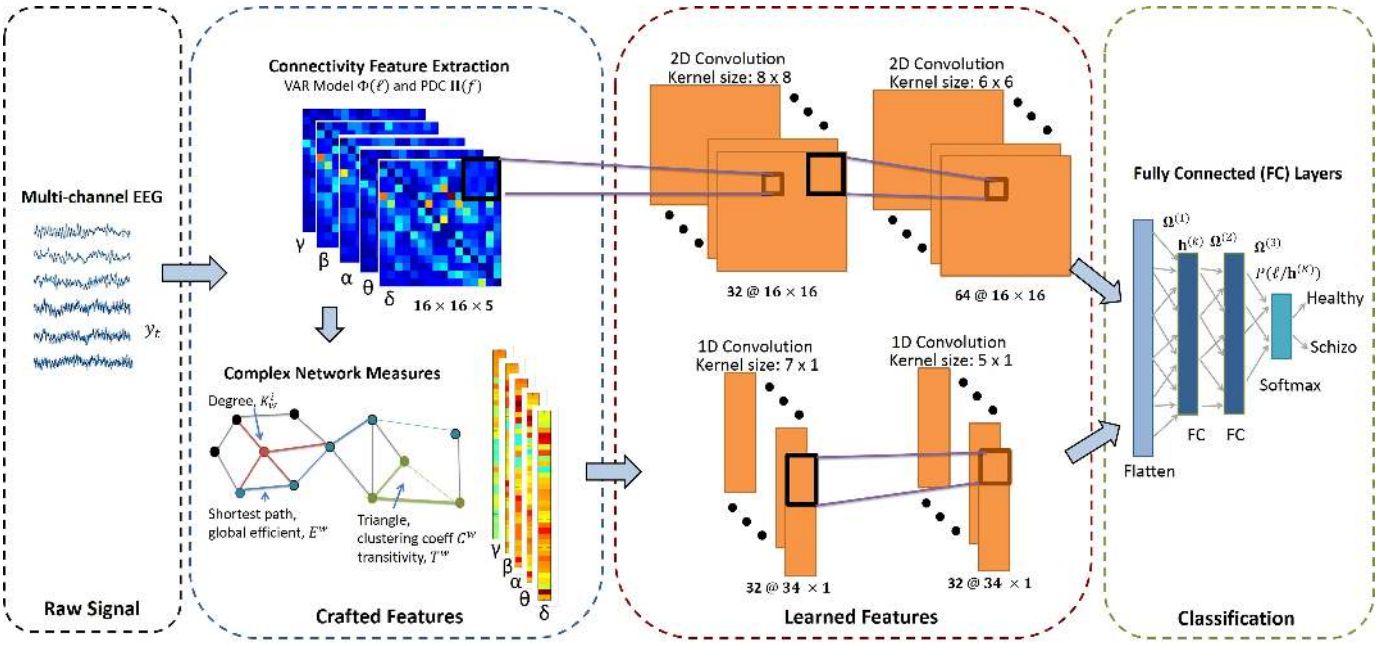

Fig. 1. Overview of the proposed MDC-CNN framework for classification of EEG-derived connectivity patterns. Brain connectome features of 2D time- and frequency-domain connectivity matrices and 1D complex network measures are estimated from multi-channel EEG signals. Using these crafted connectivity features in different domains as inputs to an ensemble of deep CNNs in parallel, high-level hierarchical feature maps are learned by multiple convolutional layers form each domain and combined before passing to classification layers.

A. Dataset

We used a publicly available SZ EEG dataset provided by the Lomonosov Moscow State University [38, 39] to evaluate the performance of proposed methods in classifying SZ and HC groups using EEG connectivity features (VAR, PDC, CN metrics and the fusion of all three feature sets). The dataset consists of 84 subjects (45 SZ patients and 39 HC), aged 11-14 years with mean adolescent age of 12 years and 3 months. Resting eye-closed EEG from 16 channels (F7, F3, F4, F8, T3, C3, Cz, C4, T4, T5, P3, Pz, P4, T6, O1 and O2 referenced to coupled ear electrodes) were recorded with sampling frequency of 128 Hz over duration of 1 minute. All SZ patients (including childhood SZ, schizotypical and schizoaffective disorders) were diagnosed at the Mental Health Research Center (MHRC), according to SZ diagnostic criteria F20, F21, F25 of ICD-10 Classification of Mental and Behavioural Disorders, set by International Statistical Classification of Diseases and Related Health Problems. Patients did not undergo any chemotherapy during examination at the MHRC.

B. Connectomic Feature Extraction

We extracted time- and frequency-domain directed connectivity measures (VAR coefficients and PDCs) and topological CN measures from EEGs.

1) Measures of Directed Connectivity: Let $\mathbf{y}_t = [y_{1t}, \ldots, y_{Nt}]', t = 1, \ldots, T$ be N-channels scalp EEG recordings over T time points. A common approach in characterizing effective connectivity between the EEG channels is through a VAR model of order L, VAR(L) on $\mathbf{y}_t$

$$\mathbf{y}_t = \sum_{\ell=1}^{L} \mathbf{\Phi}(\ell)\mathbf{y}_{t-\ell} + \boldsymbol{\epsilon}_t \tag{1}$$

where $\boldsymbol{\epsilon}_t \sim N(\mathbf{0}, \mathbf{\Sigma})$ is a white Gaussian noise with mean zero and covariance matrix $\mathbf{\Sigma} = E(\boldsymbol{\epsilon}_t\boldsymbol{\epsilon}_t')$. The directed connectivity network between different EEG channels at time lag ℓ is quantified by the $N \times N$ coefficient matrix $\mathbf{\Phi}(\ell) = [\phi_{ij}(\ell)]_{1\le i,j\le N}$. When $|\phi_{ij}| > 0$, it indicates presence of directed influence in a Granger-causality sense from channel j to channel i with strength of $|\phi_{ij}|$. Denoted by $\boldsymbol{\beta} = [\mathbf{\Phi}(1), \ldots, \mathbf{\Phi}(L)]'$ the VAR coefficients of all lags, model (1) can be written as a multivariate linear regression

$$\mathbf{Y} = \mathbf{X}\boldsymbol{\beta} + \mathbf{E} \tag{2}$$

where $\mathbf{Y} = [\mathbf{y}_{L+1}, \ldots, \mathbf{y}_T]'$, $\mathbf{E} = [\boldsymbol{\epsilon}_{L+1}, \ldots, \boldsymbol{\epsilon}_T]'$ and

$$\mathbf{X} = \begin{pmatrix} \mathbf{y}_L' & \mathbf{y}_{L-1}' & \cdots & \mathbf{y}_1' \\ \mathbf{y}_{L+1}' & \mathbf{y}_L' & \cdots & \mathbf{y}_2' \\ \vdots & \vdots & \cdots & \vdots \\ \mathbf{y}_{T-1}' & \mathbf{y}_{T-2}' & \cdots & \mathbf{y}_{T-L}' \end{pmatrix}$$

The estimators of the VAR coefficients can be computed by conditional least-squares (LS) method as $\widehat{\boldsymbol{\beta}} = (\mathbf{X}'\mathbf{X})^{-1}\mathbf{X}'\mathbf{Y}$ and $\widehat{\mathbf{\Sigma}} = (1/(T-L))(\mathbf{Y} - \mathbf{X}\widehat{\boldsymbol{\beta}})'(\mathbf{Y} - \mathbf{X}\widehat{\boldsymbol{\beta}})$.

PDC is a frequency-domain measure of effective connectivity which quantifies only the direct dependencies between nodes in a network [40]. Directed connectivity between EEG channels with oscillatory activity at specific frequency can be characterized by PDC matrix $\mathbf{\Pi}(f) = [\pi_{ij}(f)]_{1\le i,j\le N}$ with

$$\pi_{ij}(f) = \frac{|\mathbf{\Phi}_{ij}(f)|}{\sqrt{\sum_{k=1}^{N} |\mathbf{\Phi}_{kj}(f)|^2}} \tag{3}$$

where $\mathbf{\Phi}(f) = \mathbf{I} - \sum_{\ell=1}^{L} \mathbf{\Phi}(\ell)\exp(-i2\pi\ell f/f_s)$ is the Fourier transform of the VAR coefficient matrices with sampling frequency f_s. The PDC $|\pi_{ij}(f)|^2 \in [0, 1]$ is a normalized measure of the ratio between the outflow of information from channel y_{jt} to y_{it} and the total outflows of all channels from y_{jt} at frequency f.

For each subject, a VAR model (1) was fitted on the EEG

This article has been accepted for publication in a future issue of this journal, but has not been fully edited. Content may change prior to final publication. Citation information: DOI 10.1109/JBHI.2019.2941222, IEEE Journal of Biomedical and Health Informatics

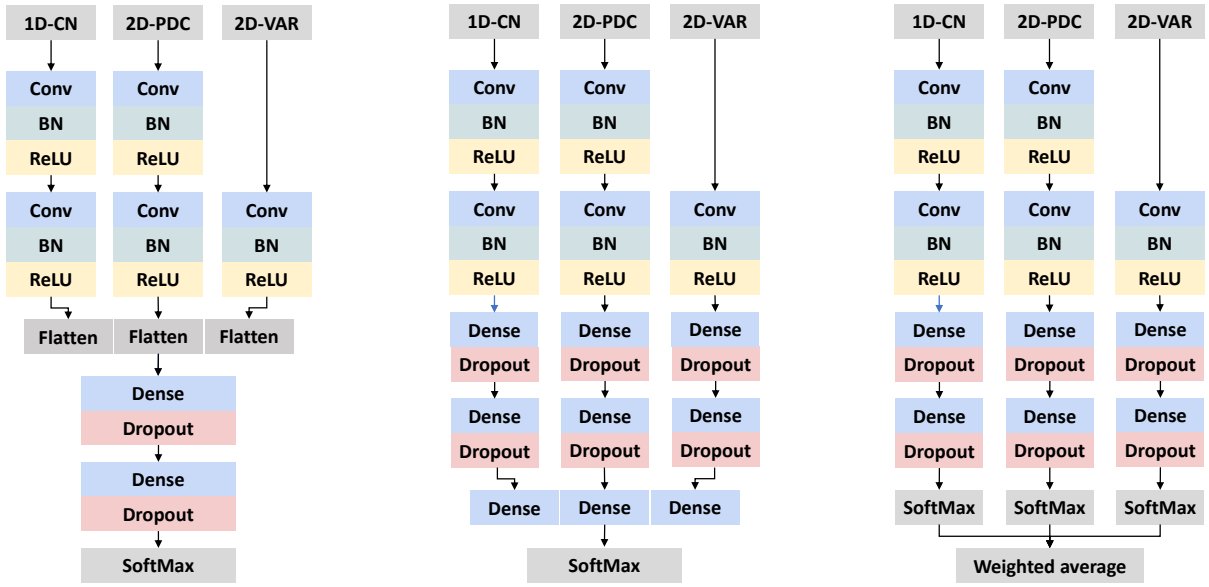

(a) Feature-level fusion (b) Score-level fusion (c) Decision-level fusion

Fig. 2. Architectures of MDC-CNN models with different fusion strategies in combining multiple domains of connectivity features. Conv: Convolution layer, BN: Batch-Normalization layer.

signals by LS and PDCs were computed from the estimated VAR coefficients as in (3). The optimal VAR model order selected by the Bayesian information criterion (BIC) averaged over all subjects was $L = 5$. Band-limited PDC matrices (self-connections excluded) were computed for five main EEG frequency bands (delta (1–4 Hz), theta (4–7 Hz), alpha (8–13 Hz), beta (14–30 Hz) and gamma (30–64 Hz)). These resulted to 3D-tensor directed connectivity (DC) features (16×16×5–lags VAR coefficients and 16×16×5–bands PDCs).

2) Complex Network Analysis: Complex network (CN) measures derived from graph theory have been widely used to characterize high-order topology of complex brain networks [19]. The CN analysis summarizes large-scale organization of brain networks into neurobiologically meaningful and easily computable measures. It could potentially reveal abnormal functional brain connectivity in psychiatric patients. Four CN measures which could reveals important information on disrupted functional integration and segregation were used to discriminate the brain network structure between SZ and healthy control. Brain network integration can be characterized by the degree and global efficiency; while the clustering coefficient and transitivity detect the network segregation.

Let $\mathbf{W} = [w_{ij}]$ be $N \times N$ weighted connectivity matrix between EEG channels, which can be quantified by the VAR coefficient matrix $\mathbf{\Phi}(\ell)$ at lag ℓ or the PDC matrix $\mathbf{\Pi}(f)$ at specific frequency f. The degree k_i^w of a node i is the total strength of weighted connections to the node, while the global efficiency measures the ease of communication between all nodes in brain network.

$$k_i^w = \sum_j w_{ij} \tag{4}$$

$$E^w = \frac{1}{N}\sum_i \frac{\sum_{j:j\neq i}(d_{ij}^w)^{-1}}{N-1} \tag{5}$$

where d_{ij}^w is the shortest weighted path length between node i and j.

The segregation of a brain network is characterized based on the number of triangles in a network. The clustering coefficient and transitivity quantify the local and global network segregation, given respectively as

$$C^w = \frac{1}{N}\sum_i C_i^w = \frac{1}{N}\sum_i \frac{2t_i^w}{k_i(k_i-1)} \tag{6}$$

$$T^w = \frac{\sum_i 2t_i^w}{\sum_i k_i(k_i-1)} \tag{7}$$

where the clustering coefficient C^w of the network is the mean of local connectivity clusters C_i^w around each node, and the weighted geometric mean of triangles around node i is computed as $t_i^w = 0.5\sum_{j,h}(w_{ij}w_{ih}w_{jh})^{1/3}$.

To quantify frequency-specific network topology, we extracted a set of complex network metrics (16 degrees, 1 global efficiency, 16 clustering coefficients and 1 transitivity) from the PDC matrix for each frequency band, giving a total of 34×5 complex network (CN) features.

C. Single-Domain CNN

In this section, we describe the generic CNN model for classifying individual connectivity feature set as a single-domain, i.e., the VAR coefficient matrices, PDC matrices, or vectors of stacked CN measures. We designed 2D-CNNs to capture spatial structure from the 16×16×5 VAR and PDC connectivity matrices across different frequency bands, and the 1D-CNN to learn the interactions between CN features. For ease of exposition and without loss of generality, we use an example of feeding the $N \times N$ PDC matrices $\mathbf{\Pi}(f)$ over five frequency bands $(\delta, \theta, \alpha, \beta, \gamma)$ as input to CNN.

CNN is a feed-forward neural network specifically designed to identify patterns in 2D images (or other 1D signals), by incorporating both feature extraction and classification

tasks. As in handling 2D-images from different color (RGB) channels in image recognition tasks, CNN can handle the 2D connectivity matrices as images and treat different time-lags or frequency bands as channels. A typical CNN consists of four layers: convolutional, activation, pooling and fully-connected (or dense) layers. In the convolutional layer, the input is convolved with a set of R kernels, added by bias terms and mapped through a nonlinear activation function to produce feature maps

$$\mathbf{h}_r = g\Big(\sum_{f\in\delta,\theta,\alpha,\beta,\gamma} \mathbf{\Pi}(f) * \mathbf{K}_r + \mathbf{b}_r \Big) \tag{8}$$

where $\mathbf{K}_r$ is the r-th 2D convolution kernel or filter (with dimension $m \times m$) and $\mathbf{b}_r$ is the bias term for $r = 1, \ldots, R$ with R is the number of filters, $*$ denotes the convolution operation in an element-wise form

$$(\mathbf{\Pi} * \mathbf{K})_{u,v} = \sum_m \sum_n \pi_{u-m,v-n} K_{u,v}$$

and $g(\cdot)$ is the element-wise activation function.

In subsequent layers, the q-th feature map of layer l is connected to R feature maps of the previous layer $l-1$ by

$$\mathbf{h}_q^l = f\Big(\sum_{r=1}^{R} \mathbf{h}_r^{l-1} * \mathbf{K}_{rq}^l + \mathbf{b}_q^l \Big) \tag{9}$$

The convolution operation offers advantage of sparse local connectivity, where each node of a layer is connected to a small localized area of the inputs. This enables detection of meaningful micro-structure features by using kernels of much smaller size than the input. Convolution layers also allow for parameter sharing where the same weights of the filter are applied across the input maps, which prevents overfitting and improves statistical and computational efficiency due to reduced number of network parameters.

Every convolution layer is often followed by a non-learnable layer called pooling, which performs sub-sampling on the feature maps by aggregating small rectangular subsets of values. Max or average pooling is applied to summarize the activation outputs within a rectangular neighborhood with a maximum or an averaged value. The pooling layers reduce the size of feature maps and enhance invariance of the features to small transitions in the input. After several convolution and pooling layers, feature maps are flattened into a feature vector, followed by a dense layer, plus a final softmax classification layer to output the predictive probabilities of class labels. The parameters of the CNN are trained by minimizing a loss function using gradient descent methods and backpropagation of the error.

D. Proposed MDC-CNN

Brain signals are complex and any analysis should capture the entire brain network using multiple classes of connectivity features. To overcome the limitations of the single-domain CNN, we develop a novel multi-domain connectome CNN model that transforms inputs of low-level VAR and PDC connectivity measures and high-level topological measures of complex brain networks to some latent hierarchical features using 2D-CNN and 1D-CNN, respectively, which are then integrated for classification decision to discriminate SZ and HC. We construct two 2D-CNNs to capture the spatial structure in the two-dimensional VAR and PDC connectivity matrices, respectively and a 1D-CNN for the CN measures of the whole-brain networks. We investigate three different fusion strategies in integrating this ensemble of CNNs trained on multiple domains of connectivity features, as shown in Fig. 2. (1) *Feature-level fusion* (in Fig. 2(a)): Feature maps from a 1D-CNN and two 2D-CNNs based respectively on the CN, VAR and PDC hand-crafted features are flattened and concatenated into a single feature vector, which is then fed into a common classification component consisting of dense layers and the softmax output layer. In the classification stage, the dense layers approximates a non-linear mapping function which further captures the interactions between the different connectivity features, followed by the softmax activation to yield the class prediction probabilities. (2) *Score-level fusion* (in Fig. 2(b)): Independent CNNs with separate convolutional and dense layers are learned for individual connectivity feature domains. The outputs from each of the domain-specific dense layers are concatenated as input to a common softmax layer for predicting the class labels. (3) *Decision-level fusion* (in Fig. 2(c)): The architecture used is similar to that in the score-level fusion. Individual domain-specific CNNs are trained separately. The predictive probability scores from the softmax layers of individual single-domain CNNs are combined via weighted averaging to generate a final decision score. The predicted class label is the one with highest weighted averaged score. The weights are learned from the training data using the naive brute-force approach. Additional results not reported here showed that using simple averaging was underperformed compared to weighted averaging. The details of configurations of the single-domain CNNs and MDC-CNNs and tuning procedure will be given in the next section.

E. Extension to Dynamic Functional Connectivity

Emerging evidence from fMRI and EEG studies has suggested dynamic changes in brain connectivity networks over time during rest or task performance, termed as the dynamic (time-varying) functional connectivity [41–43]. Recent studies also reported SZ-related aberrations in the dynamic properties of resting-state FC in fMRI [44]. The proposed MDC-CNN is well-suited only for classifying static brain networks assuming temporal stationarity of the connectivity patterns. We performed preliminary analysis of an extended framework for classifying dynamic brain connectivity based on deep recurrent neural networks (RNNs), by exploiting the temporal dynamics and dependencies in EEG-based brain networks to identify SZ. RNNs are capable of learning temporal structure in sequential patterns of variable length. Time-varying directed connectivity metrics were estimated using the widely-used sliding-window approach, in which we computed the VAR, PDC and CN measures over shifted windowed segments of EEG data, assuming locally-stationary VAR model within each temporal window. We chose a window size of 1 s (with 50% overlapping) typically used in examining dynamic connectivity in EEGs [45]. The vectorized versions of these time-evolving

TABLE I
CONFIGURATION OF 2D-CNN OF VAR CONNECTIVITY FEATURES

Layer	Type	Number	Size	Stride	Activation	Dropout
1	Input	-	16×16	-	-	0
2	Convolution	64	10×10	1	ReLU	0
3	Flattening	-	16384	-	-	0
4	Dense	512	-	-	ReLU	0.5
5	Dense	128	-	-	ReLU	0.5
6	Output	2	-	-	Softmax	0

TABLE II
CONFIGURATION OF 2D-CNN OF PDC CONNECTIVITY FEATURES

Layer	Type	Number	Size	Stride	Activation	Dropout
1	Input	-	16×16	-	-	0
2	Convolution	32	8×8	1	ReLU	0
3	Convolution	64	6×6	1	ReLU	0
3	Flattening	-	16384	-	-	0
4	Dense	512	-	-	ReLU	0.2
5	Dense	32	-	-	ReLU	0.2
6	Output	2	-	-	Softmax	0

TABLE III
CONFIGURATION OF 1D-CNN OF COMPLEX NETWORK FEATURES

Layer	Type	Number	Size	Stride	Activation	Dropout
1	Input	-	34×1	-	-	0
2	Convolution	32	7×1	1	ReLU	0
3	Convolution	32	5×1	1	ReLU	0
4	Flattening	-	1088	-	-	0
5	Dense	512	-	-	ReLU	0.2
6	Dense	64	-	-	ReLU	0.2
7	Output	2	-	-	Softmax	0

connectivity matrices were then used as input features to the RNNs.

We adopt the long short-term memory (LSTM) networks [46], an enhanced variant of RNNs to capture both the long and short-term dependencies, by using memory cell units $\boldsymbol{c}$ to store or erase temporal information with the help of their gates: *Input gates* i control whether new information should flow into the memory; *forget gates* f control whether existing information should be kept or erased from the memory; *output gates* o decide whether the current memory state should be passed to the next unit. Let $\mathbf{x}_t$, $\mathbf{h}_t$ and $\mathbf{o}_t$ denote respectively the input, hidden and output vectors at time window t. For a deep LSTM-RNN with L layers, the formulation of an LSTM unit at layer $l \in \{1, \ldots, L-1\}$ is

$$\mathbf{i}_t^l = \theta_i(\mathbf{W}_{xi}^l \mathbf{x}_t^l + \mathbf{W}_{hi}^l \mathbf{h}_{t-1}^l + \mathbf{h}_i^l) \quad (10)$$

$$\mathbf{f}_t^l = \theta_f(\mathbf{W}_{xf}^l \mathbf{x}_t^l + \mathbf{W}_{hf}^l \mathbf{h}_{t-1}^l + \mathbf{h}_f^l) \quad (11)$$

$$\mathbf{o}_t^l = \theta_o(\mathbf{W}_{xo}^l \mathbf{x}_t^l + \mathbf{W}_{ho}^l \mathbf{h}_{t-1}^l + \mathbf{h}_o^l) \quad (12)$$

$$\tilde{\mathbf{c}}_t^l = \theta_c(\mathbf{W}_{xc}^l \mathbf{x}_t^l + \mathbf{W}_{hc}^l \mathbf{h}_{t-1}^l + \mathbf{h}_c^l) \quad (13)$$

$$\mathbf{c}_t^l = \mathbf{f}_t^l \odot \mathbf{c}_{t-1}^l + \mathbf{i}_t^l \odot \tilde{\mathbf{c}}_t^l \quad (14)$$

$$\mathbf{h}_t^l = \mathbf{o}_t^l \odot \tanh(\mathbf{c}_t^l) \quad (15)$$

where $\odot$ denotes element-wise product and $\mathbf{i}_t, \mathbf{f}_t, \mathbf{o}_t, \mathbf{c}_t, \tilde{\mathbf{c}}_t$ are the input gate, forget gate, output gate, and the current and new memory cell activation vectors respectively, all have the same dimension as the hidden vector $\mathbf{h}_t$. The $\theta_i(\cdot), \theta_f(\cdot), \theta_o(\cdot), \theta_c(\cdot)$ are the corresponding activation functions. As in the CNN settings, we trained single-domain LSTM-RNNs on the estimated time-dependent VAR, PDC and CN metrics individually, and combined them to construct a multi-domain LSTM-RNN for classifying dynamic brain connectivity in SZ.

TABLE IV
CONFIGURATION OF MDC-CNN WITH FEATURE-LEVEL FUSION

Inputs	Conv	Conv	Flatten	Dense	Dense	Dropout
1D-CN	$32@5 \times 1$	$64@3 \times 1$	2176			
2D-PDC	$32@10 \times 10$	$32@8 \times 8$	8192	256	128	0.3
2D-VAR	$32@4 \times 4$	-	8192			

TABLE V
CONFIGURATION OF MDC-CNN WITH SCORE-LEVEL FUSION

Inputs	Conv	Conv	Dense	Dense	Dense	Dropout
1D-CN	$32\ @6 \times 1$	$128@4 \times 1$	64	32	2	0.2
2D-PDC	$128@5 \times 5$	$128@3 \times 8$	256	32	2	0.2
2D-VAR	$32\ @7 \times 7$	-	512	128	2	0.2

F. Model Architecture and Training

We describe the data partitioning for evaluation, configurations of the MDC-CNN, choice of hyper-parameters and the training procedure. To validate the classification performance of CNN and LSTM models, we applied a stratified five-fold cross-validation with validation and test set. The EEG recordings from all 84 subjects were randomly split into train, validation and test sets corresponding to a ratio of 6:2:2. This partition ensures no overlapping subject affiliations in the train, validation and test sets, such that the test-set contains *totally unseen* subject-oriented recordings from those in the train and validation sets.

The validation set was used in tuning the model hyper-parameters (e.g., network architecture and learning rate) where the models generalization error were measured over 200 evaluation iterations. The architecture and regularization hyper-parameters of the CNN models were optimized based on Bayesian optimization with expected improvement acquisition function [47], including the learning rate, number of convolution layers, number of filters, kernel size, MaxPooling layer, number of dense layers, number of nodes in dense layers, and dropout ratio of dense layers. The best set of hyper-parameters was selected over the five folds. For the single-domain CNNs, the optimized architectures and hyper-parameter sets of the proposed VAR-CNN, PDC-CNN and CNA-CNN models are shown in Table I, Table II and Table III, respectively. These model configurations of individual CNNs were then combined to construct the MDC-CNN model as shown in Fig. 2. For the MDC-CNNs with feature-level (Fig. 2(a)) and score-level (Fig. 2(b)) fusions, parts of models' structures were fixed as the individual CNNs, but the other hyper-parameters such as dropout values were re-optimized based on the entire network. The resulting configurations are shown in Table IV and Table V, respectively.

For performance evaluation, the new models were fitted to the combined train and validation sets based on the best hyper-parameter set and then the model performance was evaluated on the independent test set. The training of CNNs was implemented using Keras with a TensorFlow backend. Using the extracted connectivity metrics as input features, CNNs were trained using Adam optimizer [48] to update the network weights during back-propagation, with learning rates of 2.93×10^{-4}, 2.41×10^{-5} and 2.62×10^{-4} for 1D-CN, 2D-PDC and 2D-VAR models, respectively. Adam optimizer

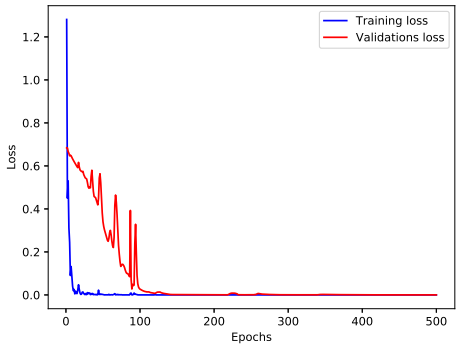

Fig. 3. The learning curve in cross-entropy loss during the training of the proposed CNN.

has been proven to be more efficient in computing stochastic gradient problem. After each convolution layer, we applied batch normalization [49] to allow the model to learn different variations of the data. Dropout [50] was also imposed on the fully-connected layers of the 2D-CNNs and 1D-CNN to increase the generalization performance of the trained models. We use rectified linear unit (ReLU) as the activation function $f(x) = \max(0, x)$ for both convolution layers and fully connected layers. To prevent information loss, we applied zero-padding to preserve the shape of features passing through convolution layers. Fig. 3 illustrates a training curve of the CNN models for PDC features, where the final epoch for early stopping of CNN training was selected based on minimal cross-entropy loss on the validation set. The feature-level and score-level MDC-CNNs were trained with learning rates of 1.55×10^{-5} and 2.21×10^{-4}, respectively. Fig. 4 shows the feature maps of the first two convolutional layers of 2D-CNN learned from the PDC matrices for the SZ and HC subjects. Apparent difference in the learned feature patterns is found between the two groups with stronger activation outputs in SZ compared to HC, particularly evident for some filters at the first layer. This suggests the ability of the proposed model to extract latent features that can discriminate between SZ and controls, and thus improving the classification performance.

For the LSTM-RNNs, the set of hyper-parameters optimized includes learning rate, number of LSTM layers, number of LSTM units, activation function, batch-normalization layer and dropout ratio. The optimized hyper-parameters are shown in Table VI, Table VII and Table VIII with learning rates of 3.76×10^{-4}, 1.17×10^{-3}, and 2.41×10^{-3} for the time-varying VAR, PDC and CN features, respectively.

III. Experimental Results

In this section, we present the SZ classification results for the proposed methods on the EEG dataset described in Section II.A. As evaluation measures, we used the classification accuracy, sensitivity, specificity and precision. These measures may be biased due to imbalance between classes, therefore we also computed modified accuracy by averaging the sensitivity and specificity *[Modified accuracy = (sensitivity + specificity) / 2]*. The correct classification due to chance is 53% due to slightly imbalanced number of subjects assigned to the two classes in test set (8 HC and 9 SZ in each fold). We compared the performance of CNNs and LSTM-RNNs with the SVM

TABLE VI
Configuration of LSTM-RNN for time-varying VAR features

Layer	Type	Size	Activation	Dropout
1	Input	118×256	-	-
2	LSTM	32	tanh	0.2
3	LSTM	32	tanh	0.2
4	LSTM	50	tanh	0.2
5	LSTM	50	tanh	0.2
6	LSTM	50	tanh	0.2
7	Output	2	Softmax	-

TABLE VII
Configuration of LSTM-RNN for time-varying PDC features

Layer	Type	Size	Activation	Dropout
1	Input	118×256	-	-
2	LSTM	32	tanh	0.3
3	LSTM	32	tanh	0.3
4	Output	2	Softmax	-

TABLE VIII
Configuration of LSTM-RNN for time-varying CN features

Layer	Type	Size	Activation	Dropout
1	Input	118×34	-	-
2	LSTM	64	tanh	0.1
3	LSTM	64	tanh	0.1
4	Output	2	Softmax	-

which has shown fairly high accuracy in classifying SZ and HC using features derived from functional connectivity maps in fMRI [32, 51].

Table IX shows the classification performance (average and standard deviation over 5 folds) for different classifiers using time-domain VAR, frequency-domain PDC, topological CN features alone in single-domain CNNs, and fusion of these features by weighted average of decision scores. We can see that CNNs clearly outperformed SVM in classifying SZ and HC EEG connectivity in all feature sets. Among the CNN models, the MDC-CNN based on the weighted-averaged fusion shows superior performance over single-domain CNNs trained on individual connectivity features alone, achieving the best accuracy of 91.69% and modified accuracy of 91.81%. It is interesting to see that VAR and PDC features performed better than network topology CN feature, indicating more discriminative information are dispersed in the whole-brain connectivity edges in the time and frequency domain compared to network topological structure as measured by the CN features. Using the topological CN features alone only achieved accuracy of 80.96% on CNN and 76.10% on SVM. High classification accuracies achieved by the single-domain CNNs suggest that each feature type may capture unique complementary aspects of the brain connectivity networks essential for discriminating HC and SZ. The proposed MDC-CNN integrating features from different domains further improves classification beyond the achievable performance from each of these feature domains individually. Nevertheless, use of LSTM-RNNs with time-varying connectivity features fails to improve over CNNs with static connectivity features. This may be due to several reasons. First, the time-varying connectivity metrics estimated based on very short windows of EEG may be less precise due to much larger number of parameters to be fitted relative to small number of observations within a window. Secondly, in contrast to directly learning the spatial patterns of 2D connectivity matrices as in CNNs, the RNNs

This article has been accepted for publication in a future issue of this journal, but has not been fully edited. Content may change prior to final publication. Citation information: DOI 10.1109/JBHI.2019.2941222, IEEE Journal of Biomedical and Health Informatics

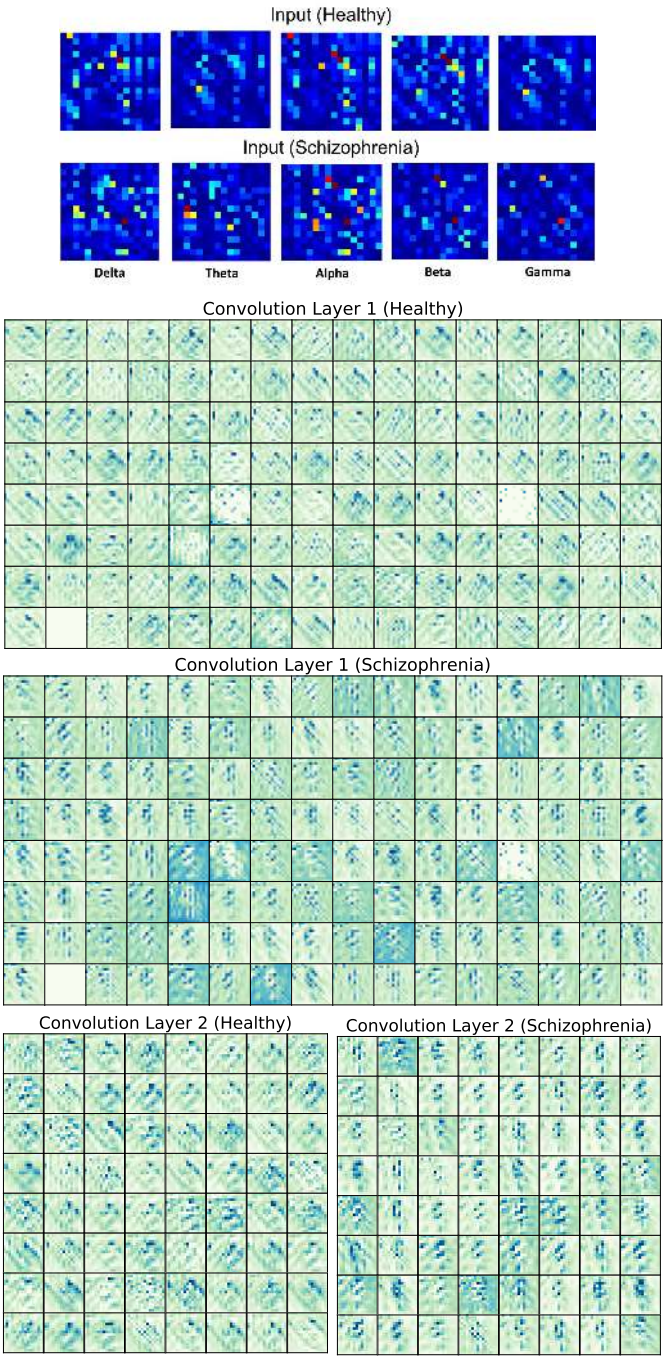

Fig. 4. Visualization of 16×16 feature maps of the first and second convolutional layers in the 2D-CNN learned from EEG-derived PDC matrices for SZ and HC subjects. 1st layer: 128 maps. 2nd layer: 64 maps.

only take vectorized inputs which neglects the spatial structure of the brain networks. Moreover, due to the inherent limitation of the RNNs that do not account for the multi-channel input patterns, we averaged the time-varying VAR and PDCs across all lags and frequency bands, which implies loss of frequency-specific information that is crucial in discriminating between the SZ and HC groups.

Table X shows the classification performance of CNN for different EEG frequency bands. The accuracy of CNN using PDC features ranged from 72.65% to 86.91% (with modified accuracy ranged from 70.95% to 86.90%), in which the alpha frequency band is more discriminative compared

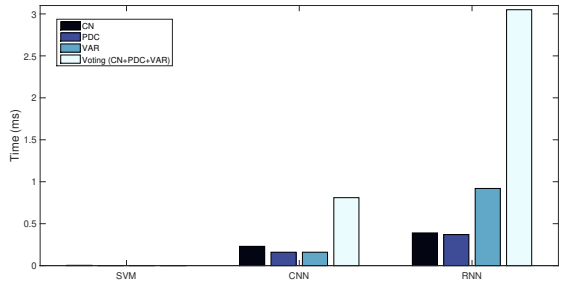

Fig. 5. Comparison of the proposed CNN and LSTM-RNNs with SVM using different connectivity features in term computational time for classification of single-subject EEG data.

to other frequency bands. This could be explained by the previous findings that the more pronounced differences in EEG connectivity between the SZ and HC were observed in the low-frequency and alpha bands [13]. Altered neural oscillation and synchronization in SZ can be associated with several key features of the disorder such as the generalized cognitive deficits, neurodevelopmental profile and cellular dysfunction [12]. On the other hand, CN features show lower average performance than PDC features in almost all frequency bands, with accuracy ranged from 58.31% to 72.50% and modified accuracy from 58.39% to 71.33%. CN features in the alpha band achieve a higher classification accuracy than the PDC, suggesting potentially more serious disruption of the brain network topology at the alpha oscillations.

We also compared the computational time required for the proposed CNN, LSTM-RNNs and SVM in classifying different connectivity features from single-subject EEG data. The classification was implemented using Intel(R) Core(TM) i7-4790 CPU at 3.60 GHz with 8 GB RAM on 64-bit Windows 7 Professional. As shown in Fig. 5, both classifiers took only fraction of seconds in identifying HC and SZ EEG connectivity. As expected, SVM performed much faster than CNN and LSTM. However, there is a trade-off between computation time and accuracy. Although the CNNs are computationally more demanding, our proposed MDC-CNN with weighted average achieved better classification accuracy compared to the best performing SVM (with weighted-average fusion), with classification time per subject of only 0.81 s.

We assessed the performance of MDC-CNNs under different fusion strategies. The results are shown in Table XI. We can see that the decision-level fusion by weighted average outperformed the other fusion schemes, despite with slightly higher computational cost for classification.

IV. Conclusion

We developed a deep CNN framework for automatic classification of SZ patients using input features based on brain connectome signatures derived from EEG. In contrast to the existing approaches, our proposed connectome CNN captures spatial structure of functional connectivity maps, leveraging information on disrupted neural connectivity patterns in SZ relative to the healthy controls for discriminative analysis at the group level. We introduced the MDC-CNN, a novel CNN architecture designed for multi-domain connectome data that can effectively combine complementary information from

TABLE IX
PERFORMANCE COMPARISON OF THE PROPOSED CNNS AND LSTM-RNN WITH SVM USING DIFFERENT EEG CONNECTIVITY FEATURES IN CLASSIFYING SZ AND HC SUBJECTS. VALUES IN PARENTHESIS INDICATE STANDARD DEVIATIONS OF PERFORMANCE MEASURES

Classifier	Feature	Dimension	Accuracy	Sensitivity	Specificity	Precision	Modified Accuracy
SVM	Time-domain (VAR)	$16 \times 16 \times 5(lags)$	85.66 (± 9.65)	86.67 (±12.96)	84.64 (± 9.29)	86.64 (± 8.28)	85.65 (± 9.49)
	Frequency-domain (PDC)	$16 \times 16 \times 5(bands)$	88.01 (± 5.52)	86.67 (± 8.31)	89.64 (± 9.48)	91.36 (± 7.35)	88.15 (± 5.50)
	Network topology (CN)	$34 \times 5(bands)$	76.10 (± 8.61)	79.29 (± 6.83)	73.33 (±11.33)	72.56 (±10.15)	76.31 (± 8.44)
	Fusion (VAR + PDC + CN)	$((2 \times 16 \times 16) + 34) \times 5$	**90.37** (± 6.31)	**91.11** (± 8.31)	**89.64** (± 9.48)	**91.64** (± 7.22)	**90.38** (± 6.27)
CNN	Time-domain (VAR)	$16 \times 16 \times 5(lags)$	89.34 (± 8.61)	86.67 (±10.89)	92.50 (±10.00)	93.14 (± 8.59)	89.59 (± 8.61)
	Frequency-domain (PDC)	$16 \times 16 \times 5(bands)$	89.19 (± 6.04)	88.89 (± 9.94)	89.64 (± 9.48)	91.64 (± 7.22)	89.27 (± 5.94)
	Network topology (CN)	$34 \times 5(bands)$	80.96 (± 4.36)	77.78 (± 9.94)	85.00 (±14.58)	87.88 (±11.19)	81.39 (± 4.72)
	Fusion (VAR + PDC + CN)	$((2 \times 16 \times 16) + 34) \times 5$	**91.69** (± 4.67)	**91.11** (± 8.31)	**92.50** (±10.00)	**94.14** (± 7.52)	**91.81** (± 4.78)
RNN	Time-domain (VAR)	118×256	76.25 (±13.83)	80.00 (±14.74)	72.14 (±18.09)	77.44 (±13.82)	76.07 (±13.96)
	Frequency-domain (PDC)	118×256	**83.38** (± 6.76)	82.22 (± 8.89)	**84.64** (± 4.87)	**85.83** (± 5.44)	**83.43** (± 6.63)
	Network topology (CN)	118×34	60.66 (± 8.19)	55.56 (±21.08)	66.07 (±16.83)	66.00 (± 9.04)	60.81 (± 7.93)
	Fusion (VAR + PDC + CN)	$118 \times ((2 \times 256) + 34)$	77.50 (±11.27)	**86.67** (±10.89)	66.79 (±14.71)	75.47 (±10.56)	76.73 (±11.23)

TABLE X
CLASSIFICATION PERFORMANCE OF CNN USING PDC AND CN CONNECTIVITY FEATURES FOR DIFFERENT EEG FREQUENCY BANDS

Feature	Frequency band	Dimension	Accuracy	Sensitivity	Specificity	Precision	Modified Accuracy
PDC	Delta	16×16	73.90 (± 4.33)	80.00 (±17.78)	66.43 (±20.68)	61.51 (± 9.05)	73.21 (± 4.11)
	Theta	16×16	76.03 (± 8.16)	80.00 (±17.78)	71.43 (±13.27)	**78.24** (±11.57)	75.71 (± 7.97)
	Alpha	16×16	**86.91** (± 4.37)	**86.67** (± 8.31)	**87.14** (± 7.94)	75.14 (±13.34)	**86.90** (± 4.33)
	Beta	16×16	80.81 (± 8.32)	**86.67** (±12.96)	74.29 (±17.74)	75.89 (±13.59)	80.48 (± 8.50)
	Gamma	16×16	72.65 (±11.45)	93.33 (± 8.89)	48.57 (±28.65)	68.72 (±11.30)	70.95 (±12.28)
	All-bands	$16 \times 16 \times 5$	89.19 (± 6.04)	88.89 (± 9.94)	89.64 (± 9.48)	91.64 (± 7.22)	89.27 (± 5.94)
CN	Delta	43×1	58.31 (±10.57)	60.00 (±34.14)	56.79 (±32.92)	50.67 (±29.38)	58.39 (±10.25)
	Theta	43×1	64.34 (± 6.14)	77.78 (±23.31)	50.00 (±37.91)	71.56 (±17.48)	63.89 (± 8.04)
	Alpha	43×1	**72.50** (± 6.64)	**84.44** (±20.61)	58.21 (±26.09)	75.01 (±13.99)	**71.33** (± 7.65)
	Beta	43×1	66.47 (±13.87)	73.33 (±33.41)	**60.00** (±40.62)	**78.59** (±19.61)	66.67 (±13.64)
	Gamma	43×1	61.84 (±11.12)	64.44 (±19.12)	57.86 (±25.12)	65.37 (±11.70)	61.15 (±11.70)
	All bands	43×5	80.96 (± 4.36)	77.78 (± 9.94)	85.00 (±14.58)	87.88 (±11.19)	81.39 (± 4.72)

TABLE XI
PERFORMANCE OF MDC-CNNS WITH DIFFERENT FUSION STRATEGIES

Performance	Feature-level	Score-level	Decision-level
Accuracy	90.44 (± 4.79)	90.44 (± 6.06)	**91.69** (± 4.67)
Sensitivity	93.33 (± 5.44)	**97.78** (± 4.44)	91.11 (± 8.31)
Specificity	89.70 (± 9.29)	81.79 (±13.24)	**92.50** (±10.00)
Precision	89.70 (± 5.83)	87.14 (± 8.39)	**94.14** (± 7.52)
Modified Accuracy	90.24 (± 4.89)	89.78 (± 6.51)	**91.81** (± 4.78)
Classification Time (sec)	0.54	0.33	0.81

multiple brain connectivity descriptors of diverse domains and dimensionality for classification purpose, including time and frequency-domain metrics of effective connectivity and complex network measures of network topology. On resting-state EEG, we demonstrated that the proposed CNN was able to learn a hierarchy of low and high-level abstract representation features from the crafted connectivity features to differentiate SZ from HC. We extend the framework to classify dynamic connectivity based on LSTM-RNNs. The proposed CNN approach gave promising classification results on a large SZ EEG dataset, outperforming traditional SVM by a large margin. The MDC-CNN with combined features also substantially improve the performance over CNNs trained on single-domain features individually, achieving the best accuracy of 91.69% using decision-level fusion. Our framework is generally applicable to other neuropsychiatric disorders besides SZ that associated with aberrant connectivity patterns and is potentially useful for development of robust computer-aided diagnostic tools in clinical settings.

There are potential limitations of this study. First, we use the generic CNNs designed for modeling image data defined on equi-spaced regular grids, which may not sufficiently capture the graph structure of brain networks. Future work could leverage on recent generalizations of CNNs to graphs [52], which can learn representations of graph-structured data lying on irregular or non-Euclidean domains and potentially improve classification of networks. While this study focuses on classifying SZ and HC, further studies could explore application of the MDC-CNN with EEG-based connectome features to automatically discriminate between SZ, schizoaffective disorder and psychotic bipolar disorder which is more difficult in differential diagnosis due to overlapping clinical symptoms [53]. Despite the effectiveness in modeling temporal dependencies in the time-varying functional connectivity, traditional fully-connected LSTM-RNNs suffers the limitation that it takes only vectorized input features which fails to preserve the spatial correlation structure in brain networks. To overcome this, [54] recently proposed an extension called the convolutional LSTM (ConvLSTM) which incorporates spatial convolutional structure in both the input-to-state and state-to-state transitions of classical LSTM, and thus may better encode the spatiotemporal correlations in the EEG data. Moreover, the proposed deep learning framework can be extended by combining the CNNs and RNNs to learn the SZ-related aberrations in both state and dynamic properties of the brain networks to improve classification accuracy.

REFERENCES

[1] M. E. Shenton, et al., "A review of MRI findings in schizophrenia," *Schizophr. Res.*, vol. 49, no. 1-2, pp. 1–52, 2001.

[2] M. R. Ho, et al., "Time–frequency discriminant analysis of MEG signals," *NeuroImage*, vol. 40, no. 1, pp. 174–186, 2008.

[3] F. B. Peter, "Neuroimaging of schizophrenia: Structural abnormalities and pathophysiological implications," *Neuropsychiatr. Dis. Treat.*, vol. 1, no. 3, pp. 193–204, 2005.

[4] G. G. Brown and W. K. Thompson, *Functional Brain Imaging in Schizophrenia: Selected Results and Methods*, pp. 181–214, Springer Berlin Heidelberg, Berlin, Heidelberg, 2010.

[5] J. Kindler, et al., "Resting-state EEG in schizophrenia: Auditory verbal hallucinations are related to shortening of specific microstates," *Clin. Neurophysiol.*, vol. 122, no. 6, pp. 1179–1182, 2011.

[6] L. V. Moran and L. E. Hong, "High vs low frequency neural oscillations in schizophrenia," *Schizophr. Bull.*, vol. 37, no. 4, pp. 659–663, 2011.

[7] K. J. Friston and C. D. Frith, "Schizophrenia: A disconnection syndrome," *Clin. Neurosci.*, vol. 3, no. 2, pp. 89–97, 1995.

[8] M. P. van den Heuvel and A. Fornito, "Brain networks in schizophrenia," *Neuropsychol. Rev.*, vol. 24, no. 1, pp. 32–48, 2014.

[9] P. Skudlarski, et al., "Brain connectivity is not only lower but different in schizophrenia: A combined anatomical and functional approach," *Biol. Psychiatry*, vol. 68, no. 1, pp. 61–69, 2010.

[10] A. Zalesky, et al., "Disrupted axonal fiber connectivity in schizophrenia," *Biol. Psychiatry*, vol. 69, no. 1, pp. 80–89, 2011.

[11] M. P. van den Heuvel, et al., "Aberrant frontal and temporal complex network structure in schizophrenia: A graph theoretical analysis," *J. Neurosci.*, vol. 30, no. 47, pp. 15915–15926, 2010.

[12] P. J. Uhlhaas, "Dysconnectivity, large-scale networks and neuronal dynamics in schizophrenia," *Current Opinion in Neurobiology*, vol. 23, no. 2, pp. 283–290, 2013.

[13] M. Maran, et al., "Electrophysiological insights into connectivity anomalies in schizophrenia: A systematic review," *Neuropsychiatr. Electrophysiol.*, vol. 2, no. 1, pp. 6, 2016.

[14] D. Lehmann, et al., "Functionally aberrant electrophysiological cortical connectivities in first episode medication-naive schizophrenics from three psychiatry centers," *Front. Hum. Neurosci.*, vol. 8, pp. 635, 2014.

[15] J. Tauscher, et al., "Low frontal electroencephalographic coherence in neuroleptic-free schizophrenic patients," *Biol. Psychiatry*, vol. 44, no. 6, pp. 438–447, 1998.

[16] G. Winterer, et al., "An association between reduced interhemispheric EEG coherence in the temporal lobe and genetic risk for schizophrenia," *Schizophr. Res.*, vol. 49, no. 1-2, pp. 129–143, 2001.

[17] J. W. Kam, et al., "Resting state EEG power and coherence abnormalities in bipolar and schizophrenia," *J. Psychiatr. Res.*, vol. 47, no. 12, pp. 1893–1901, 2013.

[18] Y. Liu, et al., "Disrupted small-world networks in schizophrenia," *Brain*, vol. 131, no. 4, pp. 945–961, 2008.

[19] M. Rubinov and O. Sporns, "Complex network measures of brain connectivity: Uses and Interpretations," *NeuroImage*, vol. 52, no. 3, pp. 1059–1069, 2010.

[20] A. Fornito, et al., "Schizophrenia, neuroimaging and connectomics," *NeuroImage*, vol. 62, no. 4, pp. 2296–2314, 2012.

[21] H. G. Schnack, et al., "Can structural MRI aid in clinical classification? A machine learning study in two independent samples of patients with schizophrenia, bipolar disorder and healthy subjects," *NeuroImage*, vol. 84, pp. 299–306, 2014.

[22] M. Shim, et al., "Machine-learning-based diagnosis of schizophrenia using combined sensor-level and source-level EEG features," *Schizophr. Res.*, vol. 176, no. 2, pp. 314–319, 2016.

[23] H. Liu, et al., "A data driven approach for resting-state EEG signal classification of schizophrenia with control participants using random matrix theory," *arXiv:1712.05289*, 2017.

[24] J. Huang, et al., "Identifying resting-state multi-frequency biomarkers via tree-guided group sparse learning for schizophrenia classification," *IEEE J. Biomed. Heal. Informatics*, pp. 1–1, 2018.

[25] Q. Zhu, et al., "Non-negative discriminative brain functional connectivity for identifying schizophrenia on resting-state fMRI," *Biomed. Eng. Online.*, vol. 17, no. 1, pp. 32, 2018.

[26] M. Sabeti, et al., "A new approach for EEG signal classification of schizophrenic and control participants," *Expert Syst. Appl.*, vol. 38, no. 3, pp. 2063–2071, 2011.

[27] E. Parvinnia, et al., "Classification of EEG signals using adaptive weighted distance nearest neighbor algorithm," *J. King Saud Univ. - Comput. Inf. Sci.*, vol. 26, no. 1, pp. 1–6, 2014.

[28] S. M. Plis, et al., "Deep learning for neuroimaging: A validation study," *Front. Neurosci.*, vol. 8, pp. 229, 2014.

[29] X. Guo, et al., "Diagnosing autism spectrum disorder from brain resting-state functional connectivity patterns using a deep neural network with a novel feature selection method," *Front. Neurosci.*, vol. 11, no. 460, 2017.

[30] A. S. Heinsfeld, et al., "Identification of autism spectrum disorder using deep learning and the abide dataset," *NeuroImage Clin.*, vol. 17, pp. 16–23, 2018.

[31] Y. Kong, et al., "Classification of autism spectrum disorder by combining brain connectivity and deep neural network classifier," *Neurocomputing*, vol. 324, pp. 63–68, 2019.

[32] J. Kim, et al., "Deep neural network with weight sparsity control and pre-training extracts hierarchical features and enhances classification performance: Evidence from whole-brain resting-state functional connectivity patterns of schizophrenia," *NeuroImage*, vol. 124, pp. 127–146, 2016.

[33] C.-R. Phang, et al., "Classification of EEG-based effective brain connectivity in schizophrenia using deep neural networks," in *Proc. 2019 IEEE Int. Conf. Neural Eng.*, 2019.

[34] A. Krizhevsky, et al., "Imagenet classification with deep convolutional neural networks," in *Advances in Neural Inform. Process. Syst.*, 2012, pp. 1097–1105.

[35] R. J. Meszlényi, et al., "Resting state fMRI functional connectivity-based classification using a convolutional neural network architecture," *Front. Neuroinformatics*, vol. 11, pp. 61, 2017.

[36] Y. Zhao, et al., "Automatic recognition of fMRI-derived functional networks using 3-D convolutional neural networks," *IEEE Trans. Biomed. Eng.*, vol. 65, no. 9, pp. 1975–1984, 2018.

[37] J. Kawahara, et al., "BrainNetCNN: Convolutional neural networks for brain networks; towards predicting neurodevelopment," *NeuroImage*, vol. 146, pp. 1038–1049, 2017.

[38] N. N. Gorbachevskaya and S. Borisov, "EEG data of healthy adolescents and adolescents with symptoms of schizophrenia," http://brain.bio.msu.ru/eeg_schizophrenia.htm.

[39] S. V. Borisov, et al., "Analysis of EEG structural synchrony in adolescents with schizophrenic disorders," *Human Physiology*, vol. 31, no. 3, pp. 16–23, 2005.

[40] K. Sameshima and L. A. Baccala, "Using partial directed coherence to describe neuronal ensemble interactions," *J. Neurosci. Methods*, vol. 94, no. 1, pp. 93–103, 1999.

[41] R. M. Hutchison, et al., "Dynamic functional connectivity: Promise, issues, and interpretations," *NeuroImage*, vol. 80, pp. 360–378, 2013.

[42] S. B. Samdin, et al., "A unified estimation framework for state-related changes in effective brain connectivity," *IEEE Trans. Biomed. Eng.*, vol. 64, no. 4, pp. 844–858, 2017.

[43] C.-M. Ting, et al., "Estimating dynamic connectivity states in fMRI using regime-switching factor models," *IEEE Trans. Med. Imaging*, vol. 37, no. 4, pp. 1011–1023, 2018.

[44] Y. Sun, et al., "Dynamic reorganization of functional connectivity reveals abnormal temporal efficiency in schizophrenia," *Schizophrenia Bulletin*, vol. 45, no. 3, pp. 659–669, 2018.

[45] F. Van de Steen, et al., "Dynamic causal modelling of fluctuating connectivity in resting-state EEG," *NeuroImage*, vol. 189, pp. 476–484, 2019.

[46] S. Hochreiter and J. Schmidhuber, "Long short-term memory," *Neural Computation*, vol. 9, no. 8, pp. 1735–1780, 1997.

[47] D. R. Jones, et al., "Efficient global optimization of expensive black-box functions," *J. Global Optimization*, vol. 13, no. 4, pp. 455–492, 1998.

[48] D. P. Kingma and J. Ba, "Adam: A method for stochastic optimization," in *Proc. 3rd Int. Conf. Learning Representations*, 2015, pp. 1–15.

[49] S. Ioffe and C. Szegedy, "Batch normalization: Accelerating deep network training by reducing internal covariate shift," in *Proc. 32nd Int. Conf. Mach. Learning*, 2015, vol. 37, pp. 448–456.

[50] N. Srivastava, et al., "Dropout: A simple way to prevent neural networks from overfitting," *J. Mach. Learn. Res.*, vol. 15, pp. 1929–1958, 2014.

[51] H. Shen, et al., "Discriminative analysis of resting-state functional connectivity patterns of schizophrenia using low dimensional embedding of fMRI," *NeuroImage*, vol. 49, no. 4, pp. 3110–3121, 2010.

[52] M. Defferrard, et al., "Convolutional neural networks on graphs with fast localized spectral filtering," in *Advances in Neural Inform. Process. Syst.*, 2016, pp. 3844–3852.

[53] Y. Du, et al., "Identifying dynamic functional connectivity biomarkers using GIG-ICA: Application to schizophrenia, schizoaffective disorder, and psychotic bipolar disorder," *Hum. Brain Mapping*, vol. 38, no. 5, pp. 2683–2708, 2017.

[54] S. Xingjian, et al., "Convolutional LSTM network: A machine learning approach for precipitation nowcasting," in *Advances in Neural Inform. Process. Syst.*, 2015, pp. 802–810.